

Development of a Skeletal Mechanism of a Four-Component Diesel Surrogate Fuel Using the Decoupling Method

Chenghan Sun, Zhongjie Shi,* Yikai Li,* Yue Lou, Gaoran Wei, and Ziming Yang

Cite This: *ACS Omega* 2023, 8, 35904–35918

Read Online

ACCESS |



Metrics & More

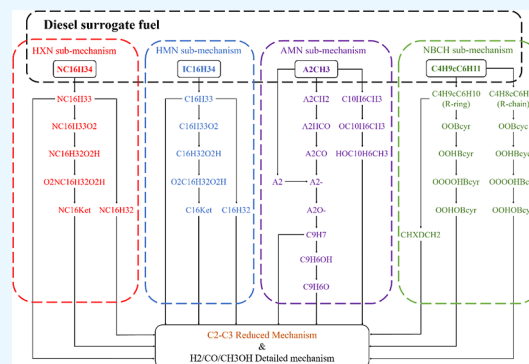


Article Recommendations



Supporting Information

ABSTRACT: Alkylcyclohexanes with a long alkyl chain account for more than 30% of diesel fuel but seldom used in the oxidation mechanism of diesel surrogate fuel due to the lack of a reduced skeletal mechanism. Hence, a four-component diesel surrogate fuel was developed with *n*-butylcyclohexane (NBCH) as the representative of alkylcyclohexanes with a long alkyl chain in real diesel. The surrogate fuel can reproduce the physicochemical characteristics of real diesel, especially the distillation range. The reduced mechanism of NBCH was developed, and the skeletal mechanism of the surrogate fuel was formulated including 80 species and 251 reactions based on the decoupling method. The mechanism was validated under a wide range of conditions with the experimental results of ignition delay time (IDT), laminar flame speed, and species concentrations of both pure components and diesel. The accuracy of the mechanism on the spray and ignition performance was further validated against the experimental data obtained in a constant volume combustion chamber system. The calculated results showed a satisfactory agreement, in which the maximum error of flame lift-off length is 7.82 mm and that of IDTs is 0.16 ms. It was proven that the mechanism is suitable to reproduce the physicochemical properties of diesel and further predict the diesel spray and ignition performance.



1. INTRODUCTION

Due to the high thermal efficiency and good reliability, diesel engines are widely used as the power source for transportation vehicles and construction machineries.^{1–3} However, the increasingly stringent emission standards have put forward higher requirements for diesel engines.⁴

In order to achieve efficient combustion and low emissions, many research studies on the effects of diesel fuel on combustion and emissions were carried out.^{5–8} Lu et al.⁹ explored the composition effects on the combustion and emission performance of two commercial diesels (China Stage-V and Stage-VI) experimentally. The main composition difference is that Stage-V diesel has a higher paraffin content and a lower naphthene content in comparison to Stage-VI diesel. It was found that the addition of decalin has a significant effect on the first-stage ignition delay time (IDT) by comparing the diesel surrogates with different compositions. Cui et al.¹⁰ built a prediction model of IDT based on the back-propagation (BP) neural network. A three-component surrogate TPRF was used, which is composed of *n*-heptane, iso-octane, and toluene. The IDT can be calculated with input parameters of ambient temperature, ambient pressure, and molar fractions. Further, with the IDT data of a real fuel at the specific temperature and pressure, the molar fraction of each component of TPRF can be acquired to match the IDT of real fuel. In addition, the application of oxygenated alternative fuels in diesel engines got more attention.^{11,12} Liu et al.^{13,14} experimentally studied the PAHs and soot formation of

diesel with oxygenated additives. It was found that the formation of A4 is consistent with soot formation. Among the oxygenated additives, *n*-butanol has the best effect on soot reduction, resulting from that the toluene content is reduced, and only small hydrocarbons like C₂H₂ and C₃H₃ are formed in the oxidation of *n*-butanol. Tan et al.¹⁵ summarized the amount of experiments on the effects of high-carbon alcohols (butanol and pentanol) blending on the combustion and emission performance of diesel engines. It was found that the low cetane number of alcohols prolongs the ignition delay, which improves the premix of fuel and air and increases the premixed combustion proportion and peak cylinder pressure. Due to the longer IDT and the oxygen content of alcohols, the soot emission of the fuel mixture is reduced. Sundar and Saravanan, and Nour et al.^{16,17} studied the effects of the blending ratio on the emission performance of diesel/hexanol in engines. The results showed that the blending ratio can reach 50% with no loss of efficiency, and the soot emission can be significantly reduced. To deeply explain the phenomenon on spray combustion, an accurate

Received: May 25, 2023

Accepted: September 8, 2023

Published: September 20, 2023



chemical kinetic mechanism of diesel needs to be developed for CFD simulation studies.¹⁸

Diesel is composed of hundreds or even thousands of hydrocarbon compounds, and the composition is extremely complex and has a certain uncertainty.¹⁹ It is almost impossible to develop a mechanism with the same composition as that of real diesel. Therefore, it is an efficient option to select some surrogates to mimic diesel fuel.²⁰ Diesel is mainly composed of four categories: *n*-alkanes, iso-alkanes, aromatics, and cycloparaffins. *N*-alkanes account for a high proportion of diesel fuel. In previous studies, some light *n*-alkanes, especially *n*-heptane, have been studied as one-component surrogate fuels due to their similar cetane number as diesel.²¹ As the carbon numbers of the main components of diesel are mainly concentrated in 10–24, the combustion characteristics of hydrocarbons with a higher carbon number have gradually become a research hotspot.^{22,23} Ranzi et al.²⁴ studied the combustion characteristics of heavy *n*-alkanes. The results showed that the chemical kinetics of *n*-alkanes are similar in a wide range of temperatures and equivalence ratio. The commonly used one-component surrogate fuels are *n*-heptane, *n*-decane, and *n*-hexadecane in recent studies.^{25,26} With the existing branched chains, the chemical kinetics of iso-alkanes are completely different from those of *n*-alkanes. It was found that with the same carbon number, iso-alkanes showed a longer IDT and lower laminar flame propagation velocity than *n*-alkanes.²⁷ Aromatics are considered as the main source of particulate matter due to the high degree of unsaturation. Aromatics did not exhibit the typical negative temperature coefficient (NTC) behavior in the experiments on IDT, which indicates that the presence of aromatics in diesel has a huge impact on the ignition performance.²⁸ Cycloparaffin, especially, alkylcyclohexane with a long alkyl chain, is one of the most important component categories in diesel, whose mass fraction is about 30–40%.²⁹ Moreover, cycloparaffin is also highly related to the polycyclic aromatic hydrocarbons and the soot formation characteristics.^{30,31} Pitz and Mueller³² summarized the development progress on detailed mechanisms of components of diesel surrogate fuels. There has been much progress on the mechanisms of *n*-alkanes, especially, large *n*-alkanes like HXN, which is in the middle of the carbon range. For iso-alkanes, the work was mainly focused on HMN. The carbon number of aromatics and cycloalkanes is lower. Especially for cycloalkanes, there are few studies on cycloalkanes with long branches, and more work is needed to increase the carbon range.

Numerous mechanisms of multicomponent diesel surrogate fuels have been developed.^{33–36} CRECK Modeling has developed a series of reduced kinetic schemes of fossil and biomass fuels.³⁷ The recent mechanism of diesel surrogates includes 201 species and 4240 reactions. The mechanism predicts IDTs, species concentrations, and laminar flame speed accurately. However, the mechanism is large, and the participation of cycloalkanes is still not considered. Lu et al.^{19,38} developed a diesel surrogate consisting of HXN/HMN/AMN and validated it by the CRECK mechanism. Further, a method for diesel surrogate formulation was built, which determined the component selection and proportion by fuel physiochemical properties and real engine performance. Bai et al.³⁹ also developed a tricomponent mechanism, consisting of HXN/HMN/AMN. The mechanism consists of 83 species and 234 reactions and reproduced the combustion and emission performance of diesel engine accurately. Chang et al.⁴⁰ developed a decoupling method for diesel surrogate formation

and conducted a four-component diesel surrogate fuel including *n*-decane, iso-octane, methyl cyclohexane, and methylbenzene. However, the carbon numbers of components are significantly less than those of the actual diesel.

In the above studies, there are few diesel surrogate mechanisms using alkylcyclohexanes with long branches as a component. In fact, the heavier alkylcyclohexane is more suitable as an alternative component of diesel than lighter alkylcyclohexane because its physical and chemical properties are closer to those of the actual fuel. Among these heavier alkylcyclohexanes, *n*-butylcyclohexane (NBCH) has a heavier molecular weight and reasonable molecular size, which is a good compromise.^{41,42} The existing oxidation mechanisms of NBCH are almost large detailed mechanisms.^{43,44} Due to the huge computation cost, it is not efficient to apply the large detailed mechanisms in engine simulation, especially in large eddy simulation (LES). The lack of a reduced mechanism has limited the further application of NBCH as one of the components of the diesel surrogate fuel in engine simulations. Therefore, reduced or skeletal mechanisms with fewer species are necessary to develop for diesel surrogate fuels.

The proportions of components are determined based on the key physicochemical properties of the diesel. The properties mainly include H/C ratio, density, molecular weight, cetane number, and distillation range.⁴⁵ Among them, the distillation range is an important parameter to characterize the evaporation performance of diesel directly. Lu et al.¹⁹ pointed out that the distillation range can reflect the working performance of diesel engine to a certain extent, especially under low-temperature conditions. However, the current mechanisms of diesel surrogate fuels did not pay enough attention to distillation ranges.

For chemical properties, the mechanisms are mainly validated by experimental data of IDT, laminar flame speed, and species concentration in the 0D model. In addition, to further verify the calculation accuracy of spray and ignition characteristics, the simulation results of engine performances, like IDT, cylinder pressure, and engine efficiency, need to be compared with experimental data. However, under engine working conditions, the in-cylinder turbulence conditions are complex, and the development of fuel spray is disturbed. The spray and ignition characteristics cannot be directly studied. The simulation in the constant volume combustion chamber (CVCC) model can effectively validate the evaporation, diffusion, and ignition performance during the development of diesel spray. However, few mechanisms of diesel surrogate fuels have been validated in the CVCC model.

In previous studies, the participation of cycloalkane, especially, alkylcyclohexanes with long branches, was almost not taken into account in diesel surrogate formation, although it is an important part of diesel. In addition, the reduced mechanism of alkylcyclohexanes with long branches is still a research blank. For mechanism validation, it mainly focuses on simulation by an engine model. Under a strong turbulence environment in the cylinder, there are too many factors that affect combustion performance, and the validation of chemical mechanisms is insufficient. In this article, the reduced mechanism of NBCH was developed, which provides a theoretical basis for the use of NBCH as a diesel surrogate component. Further, a four-component diesel surrogate fuel including 80 species and 251 reactions was developed, with the composition of HXN, HMN, AMN, and NBCH. First, the proportion of each component was calculated based on the key

Table 1. Compositions and Properties of Diesel Surrogate Fuel^{19,42}

properties	HXN	HMN	AMN	NBCX	surrogate diesel	diesel
mass fraction	35.56%	20.17%	23.00%	21.27%		
cetane number	100	15.1	0	47.6	51.65	48.9
density (kg/m ³)	756	768	986	785	817.49	837
H/C Ratio	2.13	2.13	0.91	2.00	1.76	1.77
heat of vaporization (kJ/kg)	254.05	205.79	326.32	234.59	256.8	250
lower heating value (MJ/kg)	43.95	43.85	39.35	43.42	42.76	42.70
surface tension @20°C (mN/m)	27.45	26.47	40.27	26.52	30.01	26.80
viscosity @20°C (mm ² /s)	4.40	0.89	3.47	1.60	2.88	4.22

physical properties of diesel, and the distillation range of surrogate fuel was compared with the actual diesel and other models. Then, the skeletal mechanisms of each component were developed and combined by the decoupling method. Subsequently, the mechanism was validated under a wide range of conditions with the experimental results of IDT, laminar flame speed, and species concentration. Finally, the experiments in a CVCC system were conducted under a wide temperature range, and a 3D simulation was carried out to verify the accuracy of the mechanism on the spray and ignition performance. The calculated results showed satisfactory agreement with the experimental data. It was proved that the mechanism is suitable to reproduce the physicochemical properties of diesel and further predict the diesel spray and ignition performance.

2. SURROGATE FUEL DEVELOPMENT

2.1. Decoupling Method. The decoupling methodology proposed by Chang et al.⁴⁰ was adopted to develop the present mechanism. With the decoupling methodology, the mechanism consisted of the C4-C_n scheme, the semidetailed C2–C3 mechanism, and the detailed H₂/CO/C1 mechanism. The detailed model for H₂/CO/C1 and the semidetailed model for C2–C3 are then integrated to accurately predict the laminar flame speed, heat release rate, and species concentrations, which are dominated by the oxidation kinetics of light hydrocarbons.^{46,47} The extremely simplified model for heavy hydrocarbons from C4 to C_n is constructed artificially. In the present study, the skeletal mechanisms of the components were developed, and the detailed procedure is discussed below.

For the development of a reduced mechanism, the rate constants, especially of the C4-C_n scheme, need to be adjusted. In the present study, the rate constants are mainly obtained from the existing detailed mechanisms.^{44,48–50} Because of the lumping of the isomers and the removal of reactions, the species and reactions in the C4-C_n scheme represent a series of species and reactions in the detailed mechanisms. Further, the rate constants need to be optimized to match the experimental results of IDTs, intermediates' concentration, and laminar flame speed under various conditions. The rate constants of reactions with a greater sensitivity coefficient were mainly optimized to reduce the differences. The final reaction mechanism and thermodynamic data are listed in the [Supporting Information](#).

With decoupling methodology, the mechanism consists of six blocks, HXN submechanism, HMN submechanism, AMN submechanism, NBCX submechanism, semidetailed C2–C3 mechanism, and detailed H₂/CO/C1 mechanism. The detailed H₂/CO/C1 model and the semidetailed C2–C3 model are developed based on the works of Klippenstein et al.⁵¹ and Patel et al.⁵² Bai et al.³⁹ developed a tricomponent surrogate fuel mechanism including HXN, HMN, and AMN with the decoupling method. In this study, based on Bai's³⁹ mechanism,

the reaction pathways were organized, and the reaction rates were adjusted to ensure the accuracy. As for the simplified C4-NBCX model, flux analysis and isomer-lumped methods were performed on the detailed mechanisms of NBCX sequentially, and the development of the reduced C4-NBCX scheme is discussed in the next session in detail.

2.2. Diesel Surrogate Development. To develop a diesel surrogate fuel, first, it is necessary to calculate the fraction of each component and reproduce the key physicochemical characteristics of real diesel, so as to accurately predict the evaporation and combustion characteristics of diesel. Spray and evaporation performances are mainly affected by density, viscosity, surface tension, latent heat of evaporation, and distillation range, while ignition and combustion performances are mainly affected by cetane number, adiabatic flame temperature (mainly determined by H/C ratio), and lower heating value. In conclusion, eight properties, including cetane number, density, H/C ratio, latent heat of evaporation, lower heating value, surface tension, viscosity, and distillation range, were selected as target properties. A multiproperty regression algorithm, taking the features of diesel as the target, is used to optimize the composition ratio to ensure the consistency of the key properties. The objective function of the optimization method is defined as the sum of the squared relative differences of target properties between diesel and the surrogate fuel, as expressed in eq 1⁵³

$$F = \sum_{i=1}^8 \left(\frac{p_{ic} - p_{it}}{p_{it}} \right)^2 \quad (1)$$

where p_{ic} and p_{it} are the properties of surrogate diesel and actual diesel and i is the index of the target properties. With the calculation, the composition of HXN/HMN/AMN/NBCX was confirmed, and the properties of fuels are shown in [Table 1](#).

The distillation curve of the present surrogate fuel was further compared with that of other four-component surrogate fuels in recent years and actual diesel. As shown in [Figure 1](#), it can be seen that compared with other fuels, the present fuel can reproduce the distillation performance of real diesel much better, especially for T30. In ref 19, it was pointed out that T30 can reflect the engine performances to a certain extent. T30 can not only reflect the evaporation performance but also influence the combustion rate, reflected in the maximum in-cylinder pressure and the peak heat release rate. Therefore, it can be concluded that the present surrogate fuel can predict the key physicochemical properties of diesel.

3. MECHANISM DEVELOPMENT

In this section, the development of a mechanism, especially, the extraction of the reaction path, is discussed. The main reaction

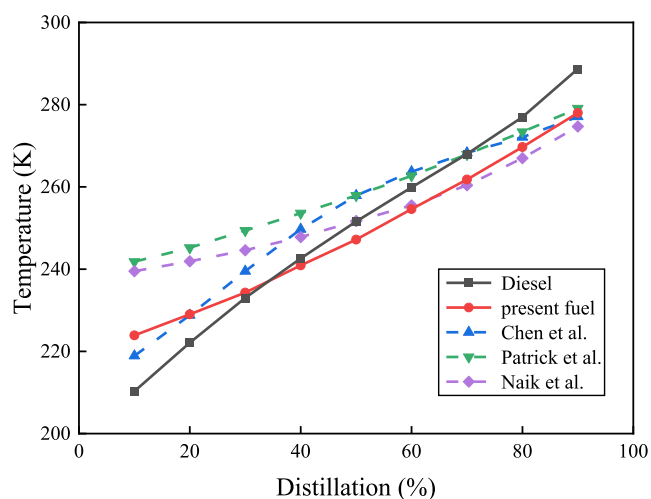


Figure 1. Comparison of distillation curves of actual diesel, the present surrogate fuel, and four-component surrogate fuels developed in recent years. (Reprinted with permission from refs 35, 54, and 55. Copyright [2018 Elsevier; 2011 Elsevier; 2017 American Chemical Society].)

pathways of the components and the blocks in mechanism are shown in Figure 2.

3.1. HXN/XMN/AMN Submechanism. HXN, HMN, and AMN are commonly used in surrogated diesel, and the skeletal mechanisms were developed maturely. The reaction pathways lumped in this study are shown in Figure 2. The reaction flows of HXN and HMN are similar. The reactions are initiated from dehydrogenation reactions to form alkyl radicals. For the low-temperature reaction path, the alkyl radicals are consumed by oxidation reactions, isomerization reactions, secondary oxidation reactions, and OH-abstraction reactions to form ketohydroperoxides. The ketohydroperoxides can decompose into active micromolecules directly. The high-temperature reactions include the decomposition reactions of alkyl radicals and the

dehydrogenation reactions of alkyl radicals, followed by decomposition reactions.

The reaction pathways of AMN are mainly initiated from the dehydrogenation reactions on both ring side and methyl side, which form C10H6CH3 and A2CH2, respectively. The O atom is added into C10H6CH3 to form OC10H6CH3. Then, OC10H6CH3 is consumed by hydrogenation reactions to form HOC10H6CH3, following which the decomposition reactions occur and micromolecules are released. For the dehydrogenation reactions on the methyl side, A2CH2 is consumed with O₂ and OH to form A2CHO. Then, the dehydrogenation reactions followed by decomposition reactions occur to produce A2-. Meanwhile, the demethylation reactions on AMN can produce naphthalene molecule A2 directly, which forms A2-. After that, naphthyl radicals are oxidized to A2O-, following which the decomposition reactions, oxidation reactions, and dehydrogenation reactions occur successively, and the micromolecules are released.

3.2. NBCH Submechanism. The existing oxidation mechanisms of NBCH are almost large detailed mechanisms.^{56–58} In this study, the reduced C4-NBCH scheme was developed based on the detailed and skeletal mechanisms reported by Mao et al.,^{44,59} which consists of 1802 species, 7246 reactions and 397 species, and 3465 reactions, respectively. Flux analysis for the stoichiometric NBCH–air mixture under 20 bar was performed to find the main pathways for NBCH oxidation, as shown in Figure 3. Eight alkyl radicals can be produced by NBCH through H atom abstraction reactions. It was found that the radicals on the alkyl chain (R1 ~ R4) and on the ring (R5 ~ R8) follow similar reaction pathways.

For high-temperature paths (red arrows), alkyl radicals decompose into smaller alkyl radicals and alkenes directly. The flux analysis was carried out to find the most important reactions in the high-temperature path, at the equivalence ratio of 1.0, pressure of 20 bar, and initial temperature of 1200 K. In Figure 3, the widths of the red arrows denote the values of production for the corresponding reactions. It can be seen that

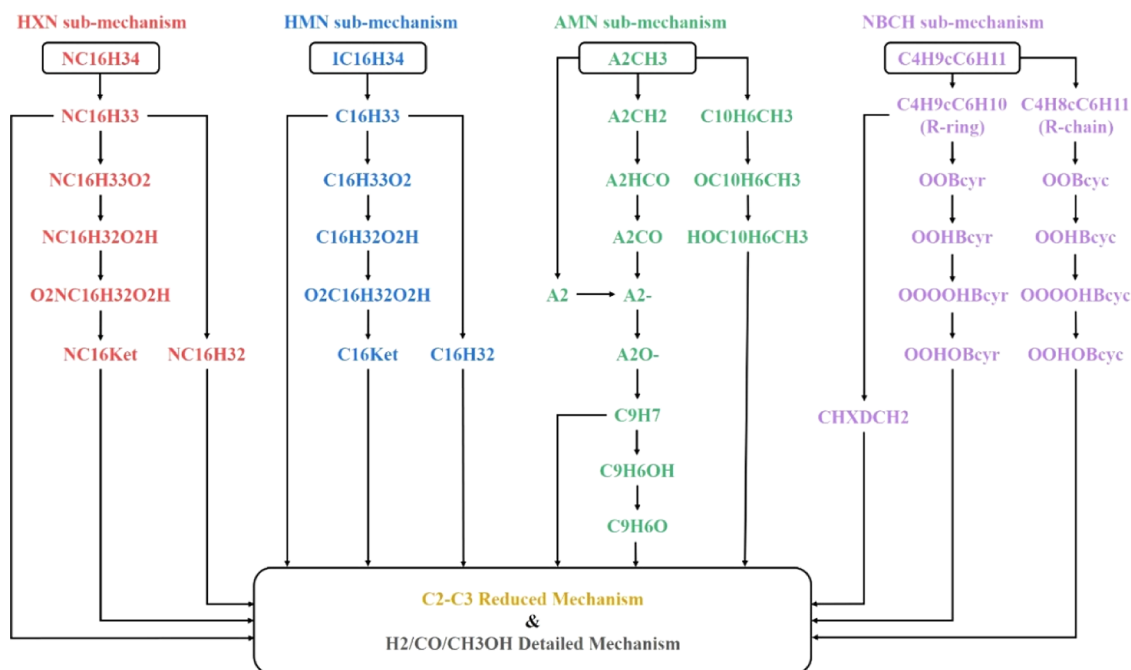


Figure 2. Main reaction pathways of the components in the diesel surrogate mechanism.

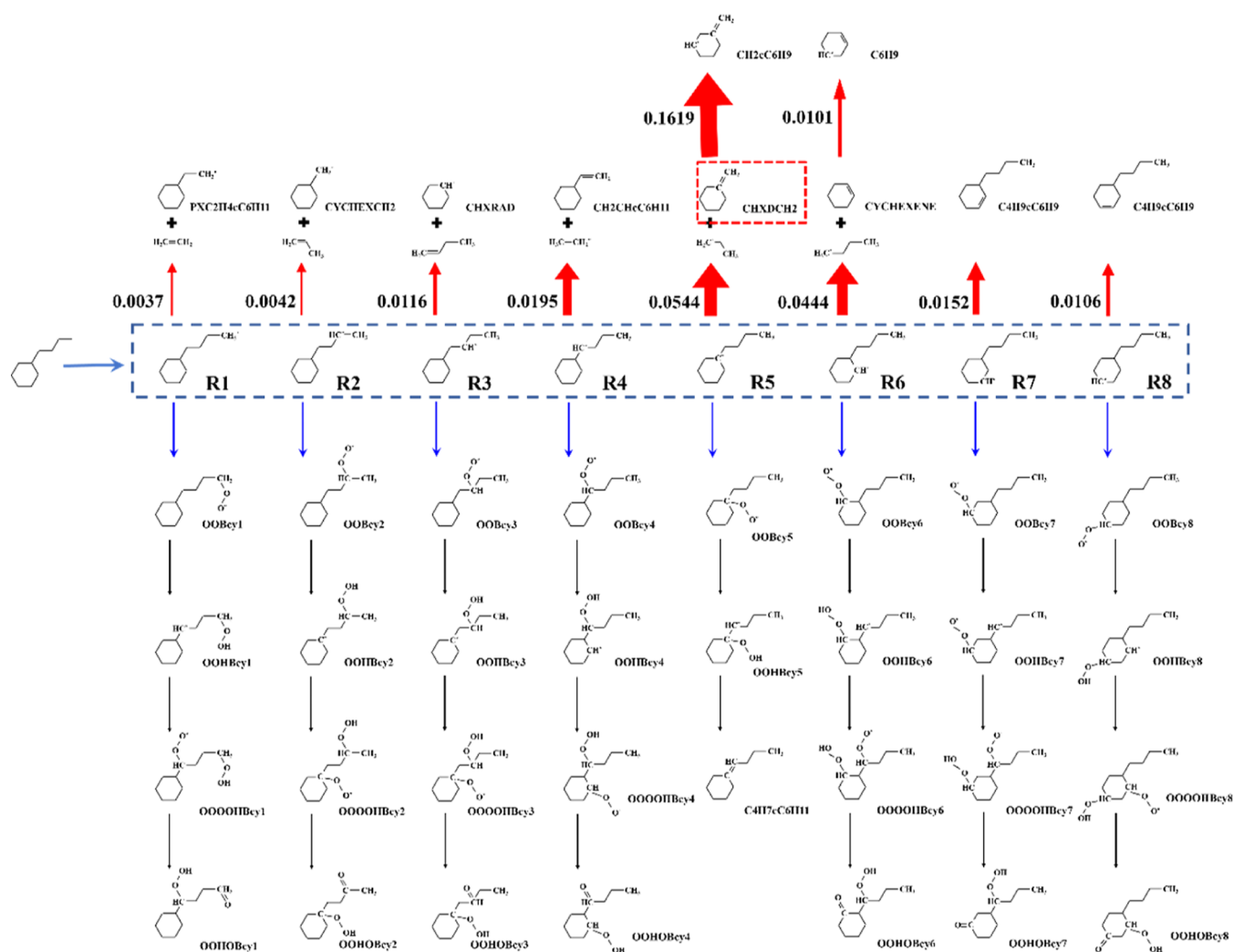


Figure 3. High-temperature (red arrow) and low-temperature (blue arrow) reaction paths for NBCH oxidation based on the initial detailed mechanism.

decomposition reactions $R5 + (M) = CHXDCH2 + C2H5$ and $R6 + (M) = CYCHEXENE + C4H9$ are the most important reactions. Therefore, conclusions can be made that at high-temperature conditions, NBCH is mainly consumed through the decomposition occurring on the ring sites. It is also confirmed in ref 44 in which the reactions of CHXDCH2 show their considerable importance on ignition in the sensitivity analyses at the temperatures of 800 and 1300 K. Hence, the high-temperature path from C4H9cC6H10 (R-ring) to CHXDCH2 was retained in the NBCH scheme.

As for the low-temperature reaction paths (blue arrows), the reaction channels are quite similar to each other for both radicals on the alkyl chain and ring. At first, the peroxy radicals (OOBcy1 ~ OOBcy8) are formed through the first O_2 addition reactions and turn into OOHBcy (OOHBcy1 ~ OOHBcy4) and OOHBcyr (OOHBcy5 ~ OOHBcy8) by isomerization reactions. Further, except for OOHBcy5, the hydroperoxyalkyl radicals are consumed through the second O_2 addition and isomerization reactions to form ketohydroperoxides (OOHOBcy and OHOBcyr) and OH radicals. According to the skeletal mechanism developed by Mao et al.,⁵⁹ at an initial temperature of 650 K, it is observed that more parent fuel is consumed to alkyl chain radicals by H abstraction reactions at low-temperature conditions. Similar phenomena can also be found

in recent works by Pitz et al.,⁴³ who concluded that RO_2 radicals are on the alkyl chain particularly isomerizing followed by the subsequent low-temperature chain branching because of the low ring strain for six-member rings. However, the sensitivity analyses in the detailed mechanism give an opposite result that the reactions in the R-ring low-temperature channel are more important at a temperature of 650 K.⁴⁴ Therefore, in the present mechanism, the low-temperature paths for the radicals on the alkyl chain and ring sites are both retained. The isomers of species in the NBCH low-temperature reaction path, including R/OOBcy/OOHBcy/OOOHBcy/OOHOBcy, were lumped. The thermodynamic data of most isomers are similar, with differences occurring mainly on sites of 1, 5, and 8. Combined with the flux analysis results, the thermodynamic data of isomers on the carbon chain were set to be consistent with the data of isomers on sites 2–4, and the thermodynamic data of isomers on the ring were set to be consistent with the data of isomers on sites 6–7.

The final reduced NBCH scheme involving 12 species and 14 reactions for low- and high-temperature chemistry was established. The above blocks were merged together, and the mechanism with 80 and 251 species was thereby obtained.

Finally, the kinetic parameters were adjusted based on the experimental IDT results. In the present study, the rate

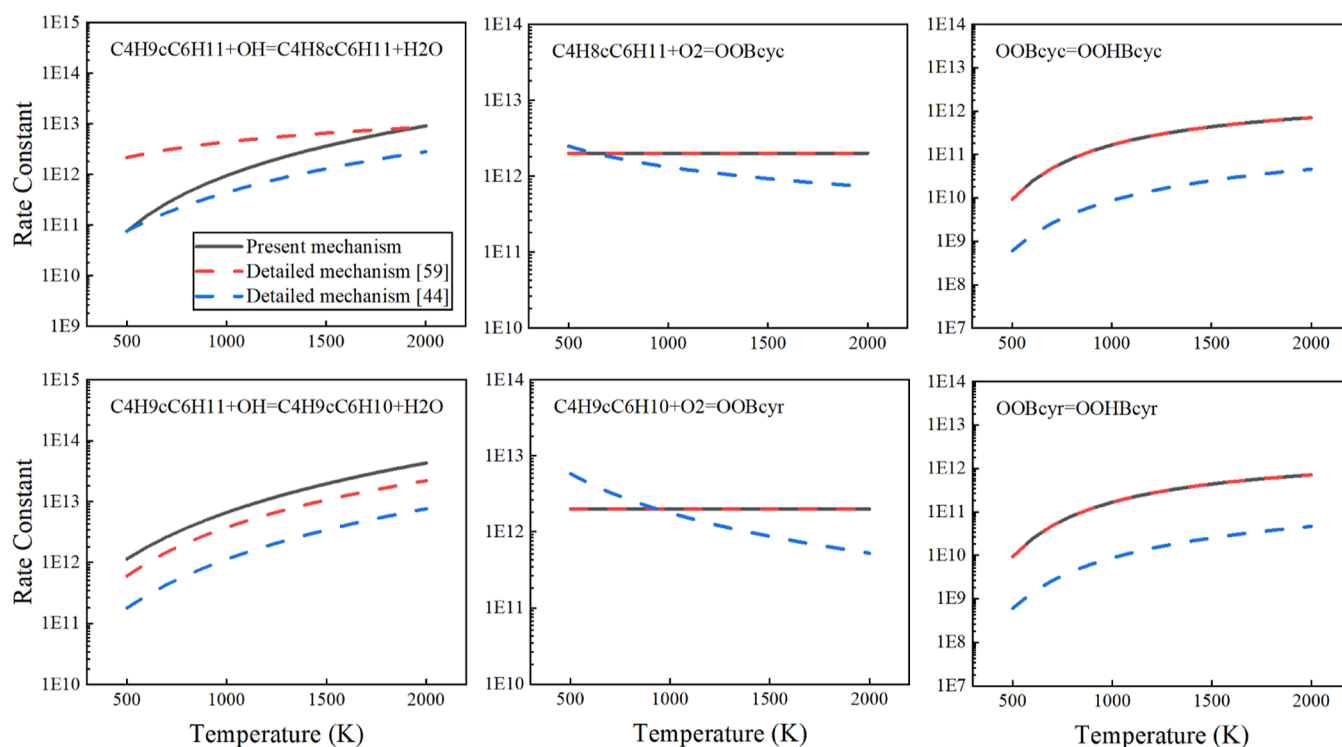


Figure 4. Comparison of reaction rate constants between the present mechanism and the detailed mechanisms. (Reprinted with permission from refs 44 and 59. Copyright [2019 Elsevier; 2019 Elsevier].)

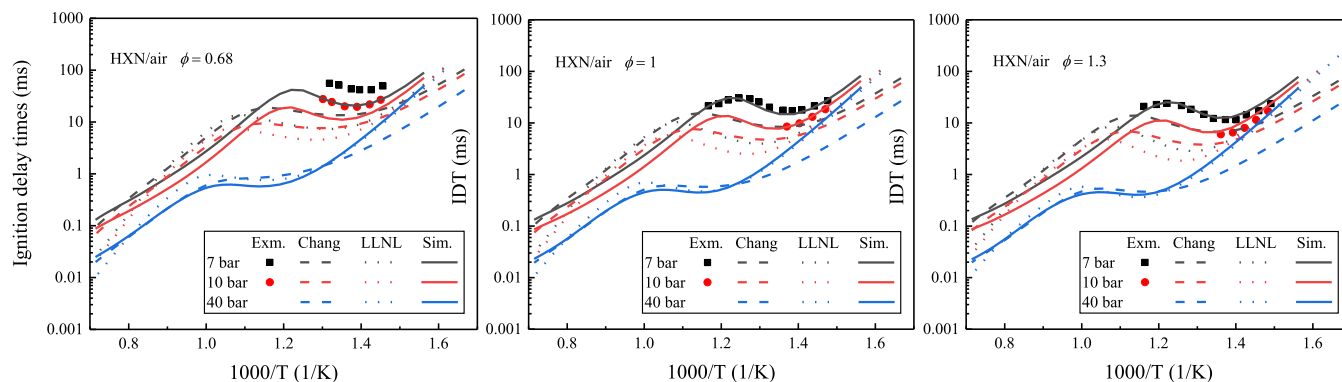


Figure 5. Comparisons of measured IDTs (scatters) and simulated IDTs of the present surrogate fuel (solid lines), Chang et al.⁴⁰ mechanism (dashed lines), and LLNL detailed mechanism (dotted lines) of HXN for $\phi = 0.68, 1,$ and 1.3 . (Reprinted with permission from refs 50, 60, and 61. Copyright [2011 Elsevier; 2013 American Chemical Society; 2017 Elsevier].)

constants were first obtained from the existing detailed mechanisms.^{44,59} Sensitivity analyses were carried out with these two mechanisms in refs 40 and 55. The results showed that the most sensitive reactions are the formation and followed isomerization of peroxy radicals (OOBcy), as well as their reverse reactions. Besides, the H-abstraction reactions of NBCH with OH also play significant roles. The optimal reaction rates are compared in Figure 4. It can be seen that there is a big gap in the rate constants of the same reactions in the detailed mechanisms developed by in refs 44 and 59. The present mechanism is mainly set consistent with the detailed mechanism in ref 59. The H-abstraction reactions of NBCH with OH were adjusted. The production reaction rate of C4H8cC6H11 was slowed down at low temperature, and the adjustment range was in the middle of the two detailed mechanisms. The production reaction rate of C4H9cC6H10 was improved in all conditions,

which is about 2 times higher than that of the mechanism in ref 59.

3.3. IDTs of Single Components. The present mechanism is first validated against the tested IDTs of single components at various pressures and equivalence ratios ϕ . Simulations are conducted using constant volume assumption at the same conditions with the tests, while the temperature range is extended. The simulated IDT is defined as the time at which the slope of the temperature profile reaches its maximum value.

As shown in Figure 5, for IDTs of pure HXN, the calculated results of the present mechanism were compared with those of other detailed mechanisms^{50,60} and the experimental data.⁶¹ The experimental results are mainly obtained at low temperature, and the calculated results of the detailed mechanisms are obviously lower than the experimental results. By adjusting the rate constants of low-temperature reaction pathways, the present mechanism can achieve better reproduction of

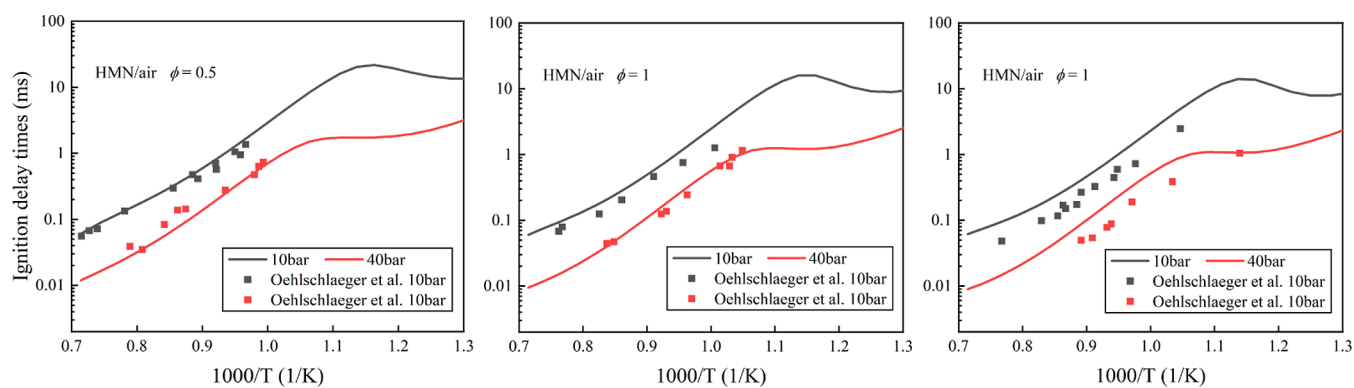


Figure 6. Comparisons of measured (scatters) and simulated (solid lines) IDTs of HMN for $\phi = 0.5, 1,$ and 1.5 . (Reprinted with permission from ref 49. Copyright [2009 Elsevier].)

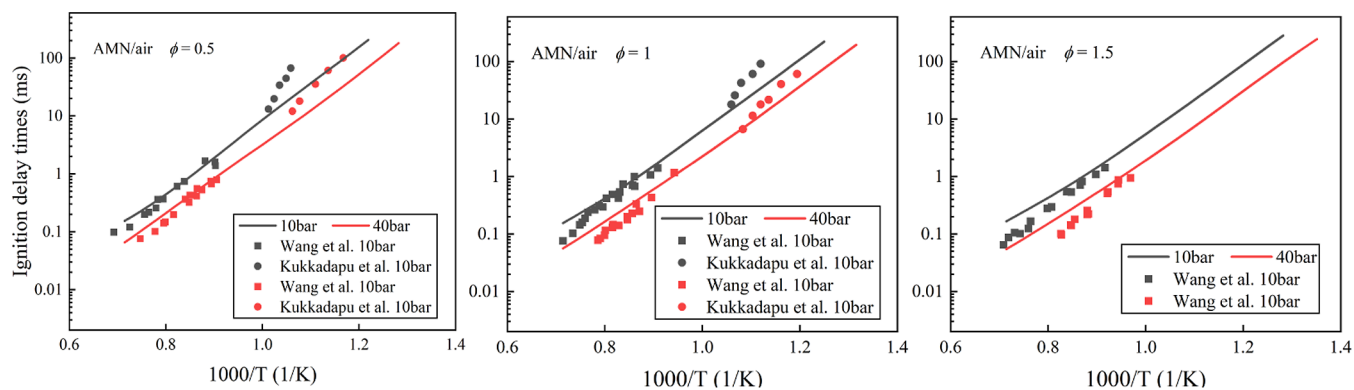


Figure 7. Comparisons of measured (scatters) and simulated (solid lines) IDTs of AMN for $\phi = 0.5, 1,$ and 1.5 . (Reprinted with permission from refs 48 and 62. Copyright [2010 Elsevier; 2017 American Chemical Society].)

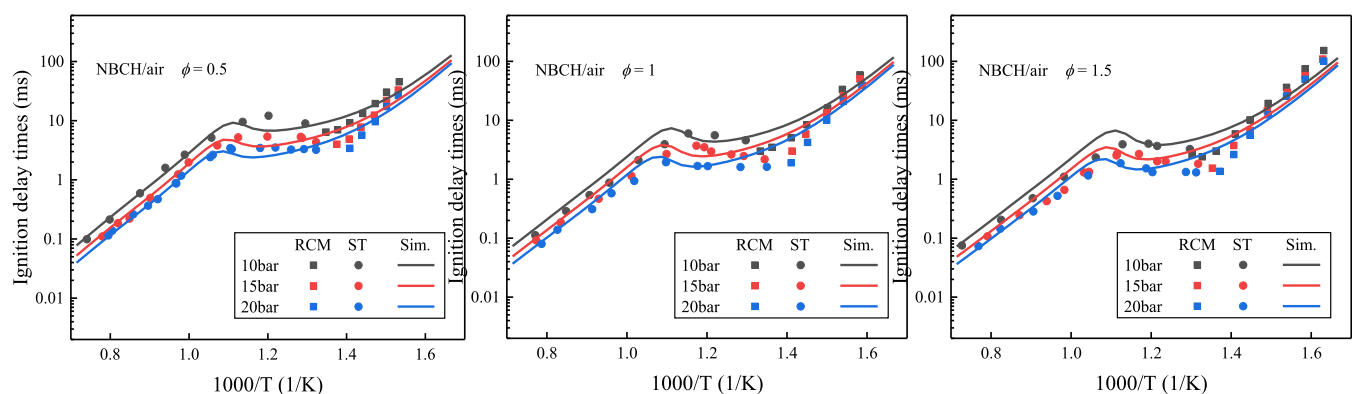


Figure 8. Comparisons of measured (scatters) and simulated (solid lines) IDTs of NBCH for $\phi = 0.5, 1,$ and 1.5 . (Reprinted with permission from ref 59. Copyright [2019 Elsevier].)

experimental data under low temperature conditions. Meanwhile, the calculated data are close to those of the detailed mechanisms under high-temperature conditions. In addition, the temperature of the NTC region is also consistent with the experimental data. Under low-pressure conditions, the high-temperature limit of the NTC region is slightly lower than that of the detailed mechanisms.

The experiments on IDT of HMN are mainly conducted under high-temperature conditions.⁴⁹ As shown in Figure 6, under various equivalence ratios and pressures, the calculated results agree well with the experimental data. Especially under $\phi = 1.5$, the present mechanism can accurately predict the NTC phenomenon of HMN. For AMN in Figure 7, the calculated

data is in good agreement with the experimental results.^{48,62}

There is no NTC phenomenon in the experimental and calculated results.

Compared with experimental data,⁵⁹ it can be seen in Figure 8 that the present mechanism reproduces this behavior of IDT of NBCH depended on the pressure and temperature under different equivalence ratios. Overall, the present mechanism can reproduce the measured IDTs of pure components satisfactorily at a wide range of temperatures, pressures, and equivalence ratios.

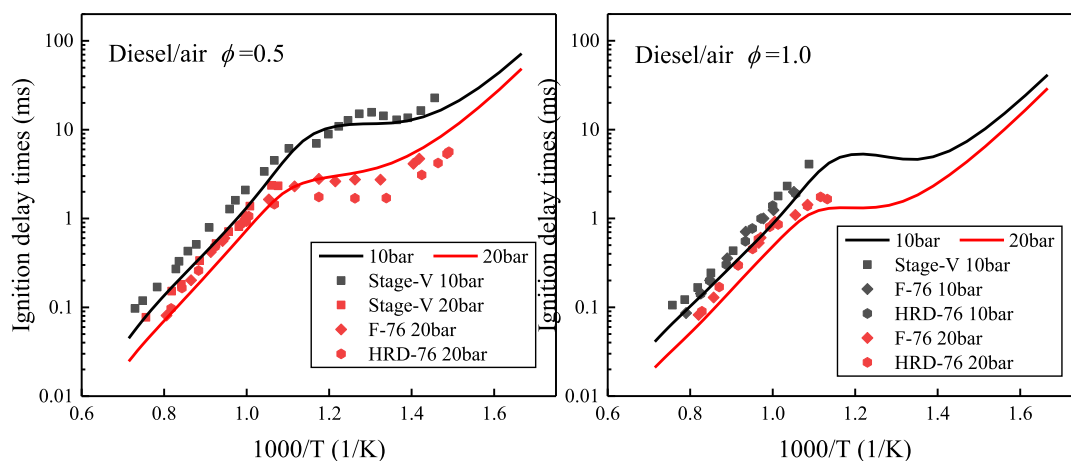


Figure 9. Comparisons of measured (scatters) and simulated (solid lines) IDTs of diesel. (Reprinted with permission from refs 9, 63, and 64. Copyright [2019 Elsevier; 2014 Elsevier; 2019 Elsevier].)

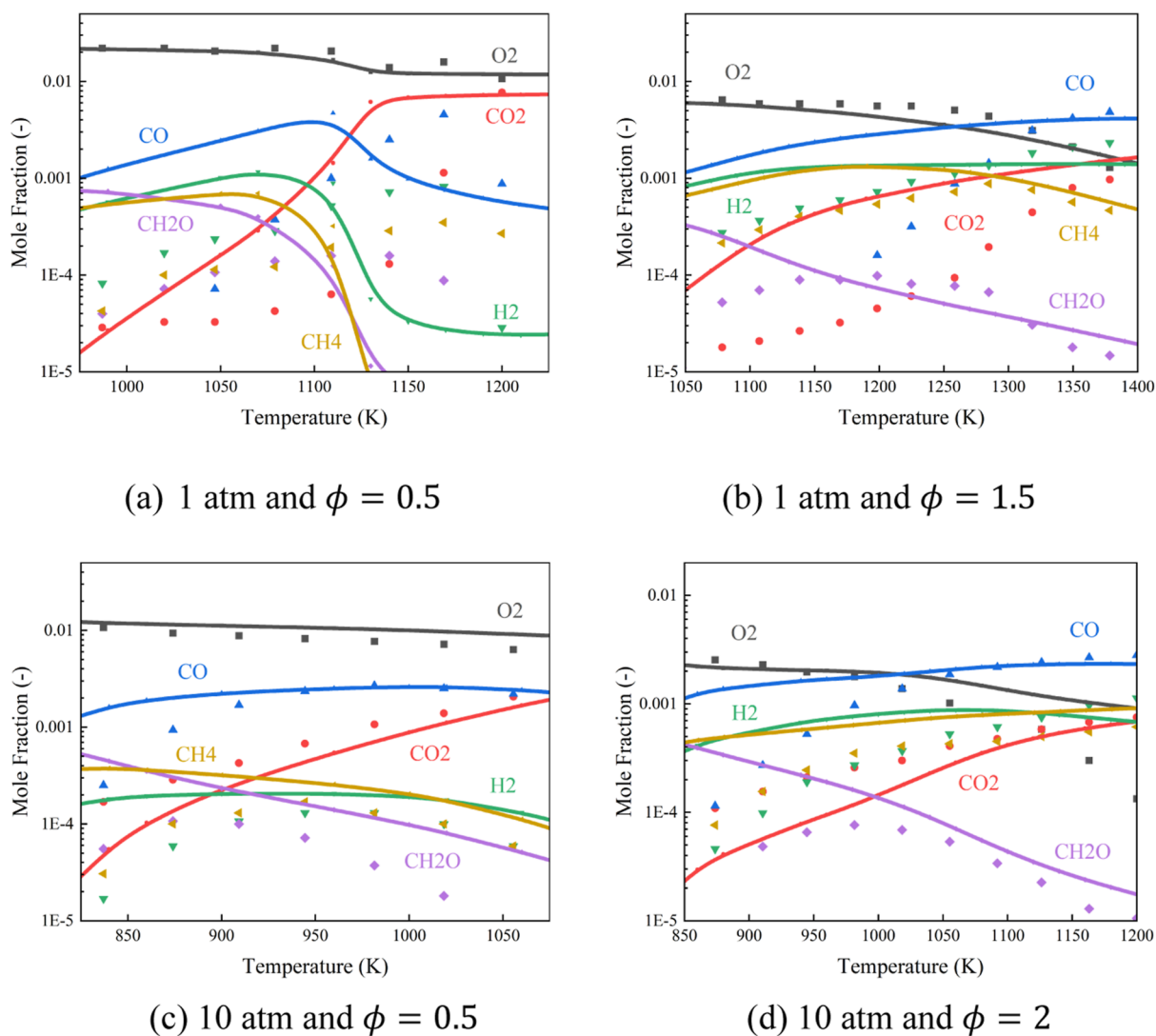


Figure 10. Comparisons of measured and simulated intermediate concentrations of diesel under (a) 1 atm and $\phi = 0.5$; (b) 1 atm and $\phi = 1.5$; (c) 10 atm and $\phi = 0.5$; and (d) 10 atm and $\phi = 2$. (Reprinted with permission from ref 65. Copyright [2007 Elsevier].)

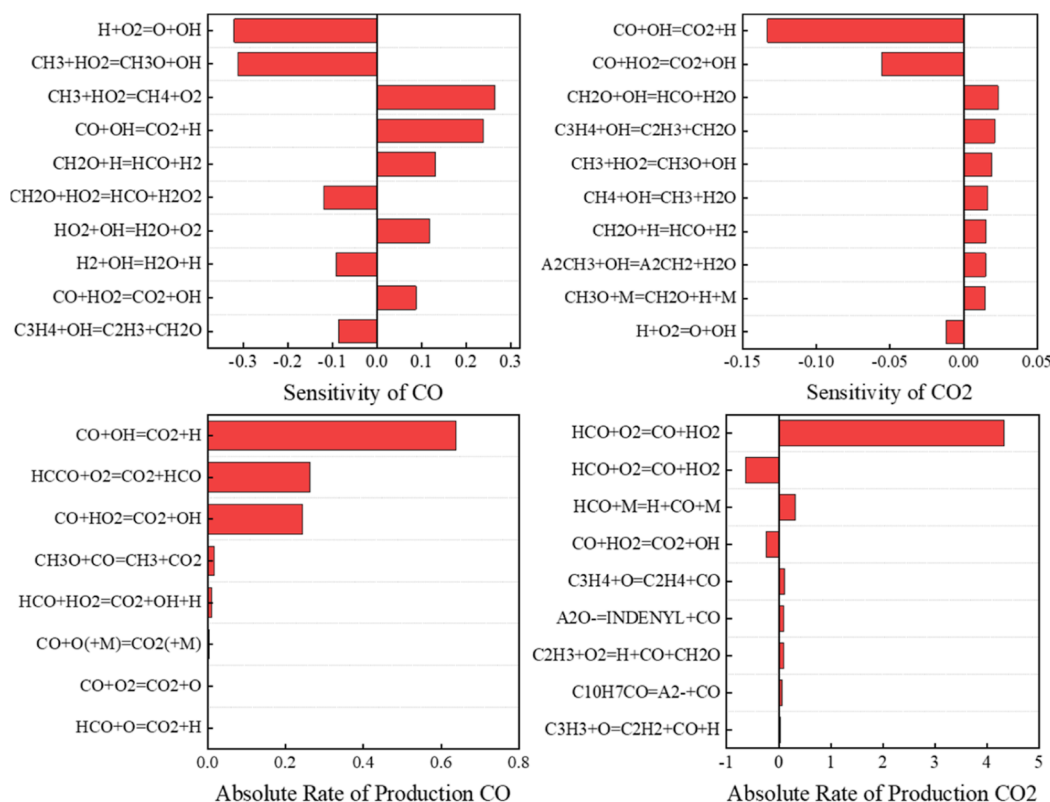


Figure 11. Rate of production and sensitivity analysis for CO and CO₂ under 1 atm and $\phi = 0.5$.

4. RESULTS AND DISCUSSION

The mechanism was validated with experimental data of single components and diesel. The simulations were conducted by CHEMKIN-PRO software. Finally, the 3D simulation of diesel spray was conducted with CONVERGE software and validated with experimental results under a wide range of temperature conditions.

4.1. 0D Validations for Diesel/Air Mixture. 4.1.1. Ignition Delay. The IDTs of real diesel were further validated for the accuracy of the mechanism. As shown in Figure 9, the calculated IDTs under equivalence ratios of 0.5 and 1, pressure of 10 and 20 bar, were compared with the experimental results of various types of real diesel.^{9,63,64} The calculated results agreed well with the experimental data, and especially, under an equivalence ratio of 0.5, the NTC region was reproduced accurately.

4.1.2. Species Concentrations. Figure 10 shows comparisons between the measurements and simulations for the concentrations of intermediates under different pressures and equivalence ratios. The trend of mole fraction of each intermediate is well predicted. The calculated O₂ mole fraction is consistent with the experimental data, indicating that the prediction of the reaction process is accurate. However, in Figure 10a, the predicted peak of CO appears at 1120 K, while the experimental data are 1170 K. In addition, for the curves of other species, there are also shifts of about 50 K in advance. It shows that under low-pressure conditions, the present mechanism overpredicts the reaction rate a little. Under this condition, the rate of production and sensitivity analysis for CO and CO₂ were conducted. As shown in Figure 11, the C0–C1 submechanism has the highest influence on CO₂, and the submechanism of C2–C3 and A2CH3 also have certain effects on CO₂. It indicates that the discrepancies between tests and modeling are attributable to inaccuracies in the C0–C1

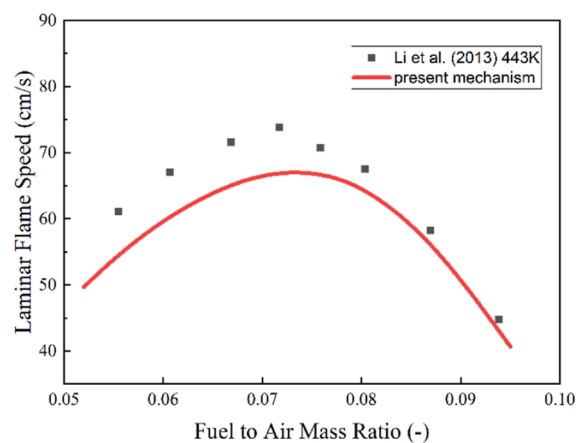


Figure 12. Comparison of measured and simulated laminar flame speed of diesel. (Reprinted with permission from ref 66. Copyright [2013 Elsevier].)

submechanism, and the accuracy of the C2–C3 submechanism and the A2CH3 submechanism also needs to be further improved.

4.1.3. Laminar Flame Speed. Figure 12 shows the comparison between the measurements and simulations for the laminar flame speed of diesel. It can be found that the present reduced chemistry predicts the laminar flame speed better at a high equivalence ratio. The dependence of laminar flame speed on the fuel-to-air mass ratio is predicted well. The experimental error is about 5 cm/s,⁶⁶ and the biggest difference between experimental data and present simulation results is 7.05 cm/s, which is a reasonable error within 10%.

Figure 13 shows the sensitivity analysis result of the laminar flame speed. Similar to species concentration results, the C0–

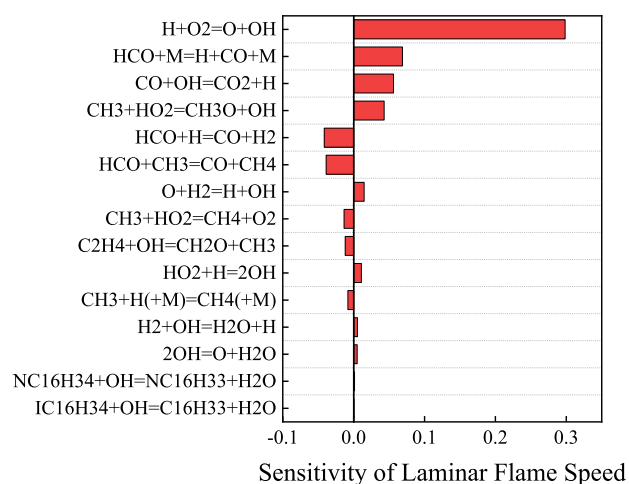


Figure 13. Sensitivity of the laminar flame speed with a fuel-to-air mass ratio of 0.655.

C1 submechanism also has the highest influence on laminar flame speed. Hence, for the present lumped mechanism, the prediction error of laminar flame speed is mainly resulted from the oversimplified C0–C1 submechanism. The authors have admitted that their reduced model has some problems in

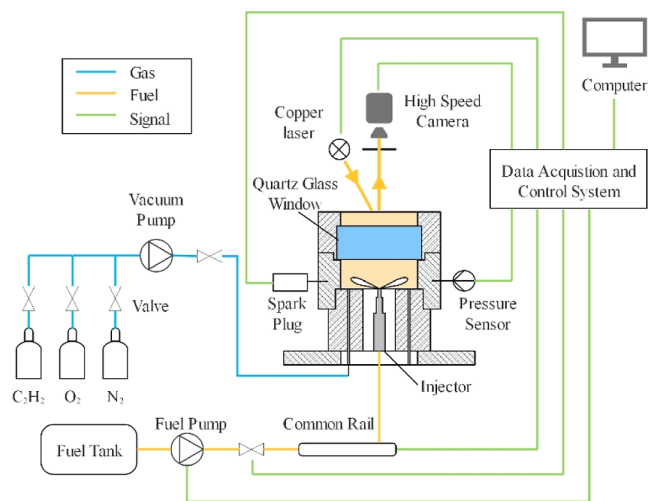


Figure 14. Schematic of the experimental apparatus.

predicting the laminar flame speed in the revised manuscript and will improve it in the future study.

4.2. 3D Validations for Diesel Spray Autoignition.

4.2.1. Experimental Method. The schematic of the experimental apparatus is shown in Figure 14. The experimental system mainly includes a CVCC with a bore of 110 mm and a height of 65 mm, fuel supply system, ignition system, data acquisition system, and high-speed photography system. The Phantom V7.1 high-speed camera was set directly above the chamber. The ambient density in the chamber is set at 15 kg/m³, and the oxygen concentration is set at 21%. A six-hole injector with 0.12 mm orifice diameter was mounted at the center of the bottom of the chamber. The injection pressure was set at 80 MPa by a common rail system, and the fuel temperature was 293 K. In the present study, the liquid penetration length (LPL) and ignition features are obtained simultaneously, and the luminosity IDT data was obtained based on picture process-

ing.^{67–69} According to the results of ref 67, the peak in the total intensity increment curve by the Schlieren image processing has a good match with the high-temperature ignition. The experimental flame lift-off length (LOL) is defined as the axial distance from the luminous area to the nozzle for the steady flame. Three times of duplicate tests were conducted under one condition, and the average IDTs were obtained. A detailed

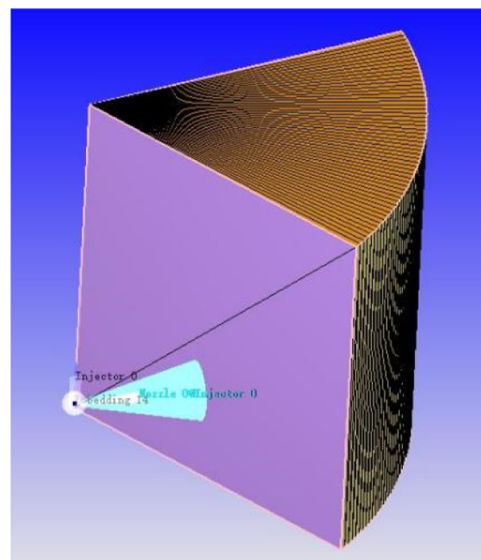


Figure 15. Simulation model of the 1/6 model.

description of the experimental setup was described in our previous work.⁷⁰

4.2.2. Spray Validation. In the present study, the simulation model was created based on the experimental set. As the chamber and injector have a symmetric structure, a 1/6 chamber model with one injector hole was built, as shown in Figure 15. The grid was generated internally with CONVERGE software. The base grid was fixed at 1 mm. To obtain the details of the flow field near the injector, a fixed embedding containing the spray range was used with a minimum grid of 0.25 mm. The adaptive

Table 2. Submodel Options in CONVERGE

submodel	
turbulence model	dynamic structure ⁷²
spray breakup model	Kelvin–Helmholtz ⁷³ and Rayleigh–Taylor ⁷⁴
combustion model	SAGE ⁷⁵

mesh refinement with three levels was permanently employed during the simulation for the velocity field, the temperature field, and the key species (CH₂O and OH) mass fraction field. In the computational domain, the minimum grid was 0.125 mm, which is suitable to ensure the accuracy of the calculation of LES turbulence model.⁷¹ The submodel options are listed in Table 2.

The spray performance was validated by LPL in a reacting model. The simulated LPL is defined as the maximum axial distance from the nozzle to the farthest position corresponding to 90% fuel mass. The validation results are shown in Figure 16. The calculated LPLs remain in the range of experimental data under different temperatures. The red dots are the measured LPLs in the repeated tests. It can be seen that the calculated value is always within the experimental measurement range. It

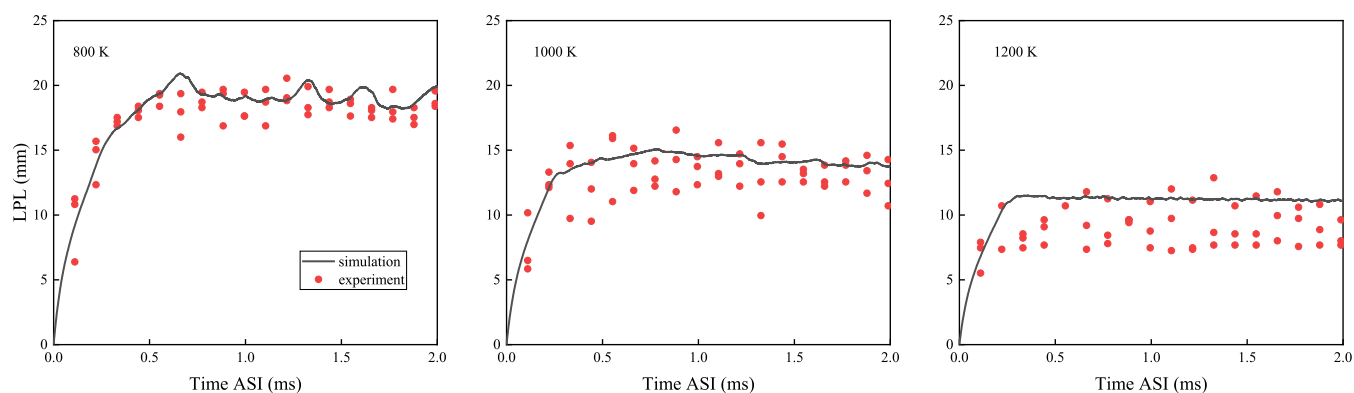


Figure 16. Comparisons of LPLs between measured and simulated values at different temperatures.

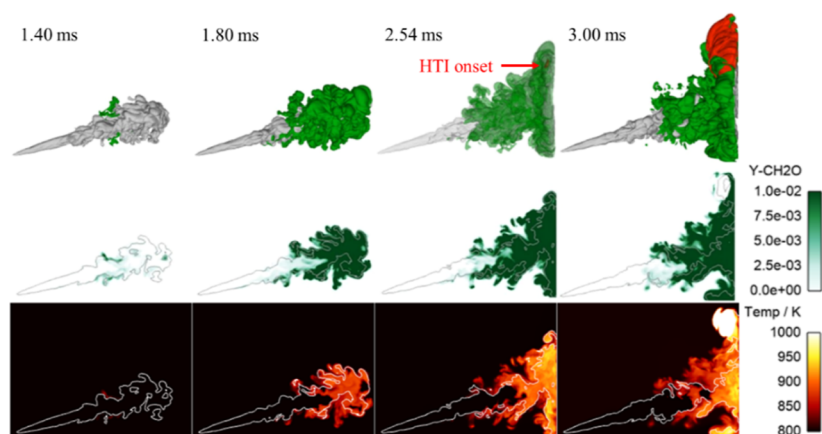


Figure 17. Spatiotemporal evolution of spray development and ignition process at an ambient temperature of 800 K, with the $Y\text{-CH}_2\text{O}$ and temperature distribution on the center plane of the pure diesel spray. In the first row, the $\phi = 1$, $Y\text{-CH}_2\text{O} = 1 \times 10^{-2}$, and $Y\text{-OH} = 5 \times 10^{-5}$ isosurfaces are represented by gray, dark blue, and red surfaces, respectively. While in the second and third row, the $\phi = 1$ isolines are supposed on the $Y\text{-CH}_2\text{O}$ and temperature distributions to show the spray evolution.

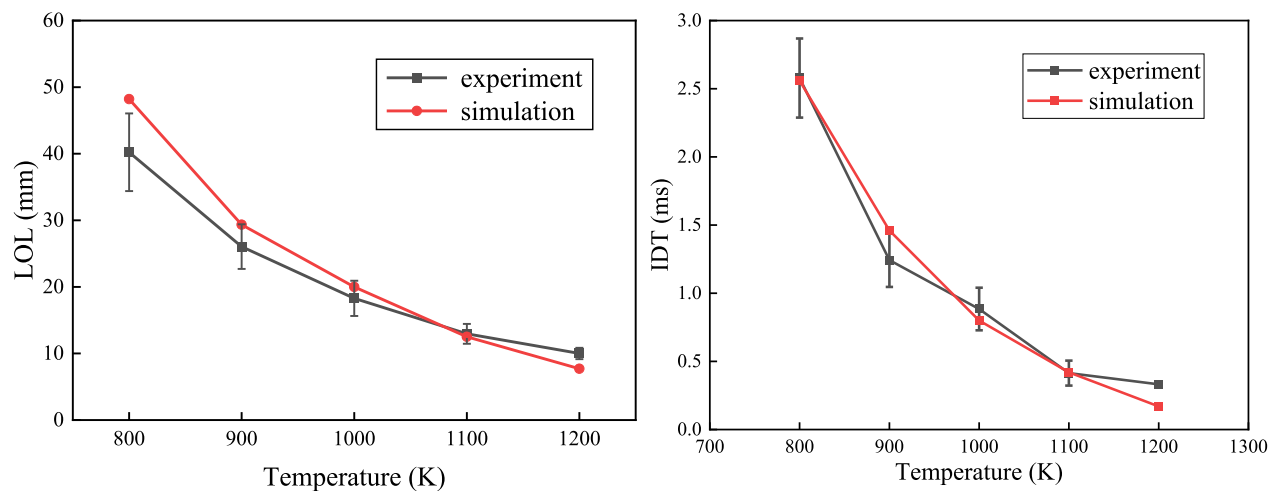


Figure 18. Comparison of measured and simulated LOLs and IDTs in a diesel spray model under different temperatures.

rises at the initial stage of injection and then remains at a stable value.

4.2.3. Comparisons of IDTs and LOLs. The spray ignition is divided into two processes, including low-temperature ignition (LTI) and high-temperature ignition (HTI), and CH_2O and OH are defined as the representatives, respectively. The rapid generation of OH represents the onset of HTI. The simulated IDT is defined as the time at which the OH mass fraction reaches

2% of the maximum in the domain after a stable flame is established as the ECN standard. In the present study, an OH mass fraction of 5×10^{-5} is used as the threshold of HTI. Correspondingly, the simulated LOL is defined as the axial distance from the nozzle to the position with an OH mass fraction of 5×10^{-5} when the flame is stabilized.

The first row of Figure 17 depicts the spatiotemporal evolution of spray, while the second and third rows show the

Y-CH₂O and temperature distribution evolutions on the center plane. In the first row, the $\phi = 1$, Y-CH₂O = 1×10^{-2} , and Y-OH = 5×10^{-5} isosurfaces are represented by gray, dark blue, and red surfaces, respectively. While in the second and third row, the $\phi = 1$ isolines are supposed on the Y-CH₂O and temperature distribution to show the spray evolution.

As shown in Figure 17, CH₂O is first generated at the radical periphery of the spray at 1.40 ms, mainly concentrated at the region $\phi < 1$. At the corresponding region in the third row, it can be seen that the onset of low-temperature reactions (LTRs) is followed by a little heat release. This observation shows that the LTRs are first induced at the periphery of the spray, where the local temperature is high due to higher entrainment of the high-temperature air. With the LTRs proceeding, the Y-CH₂O increases and penetrates to the inner area of spray head. Also, the simulation result that LTRs start from the periphery of the spray and then penetrate to the inner area of spray head is consistent with the experimental results conducted in refs 76–7778. At 2.54 ms, it can be seen that OH is generated at the rich side of the $\phi = 1$ isosurface at downstream of spray. These modeling results are consistent with the 2D DME mixing layer study of Krisman et al.⁷⁹ and the direct numerical simulation of *n*-dodecane spray by Dalakoti et al.,⁸⁰ who showed that the HTRs preferentially occur in rich mixtures. With high-temperature reactions (HTRs) proceeding, at 3.00 ms, it is obvious that the HTRs take place with the rapid consumption of CH₂O and high-level heat release. Generally, the present diesel surrogate fuel is competent to capture both the low- and high-temperature autoignition processes in the diesel spray.

The comparisons of LOLs and IDTs with experimental data under different temperatures are listed in Figure 18. While both the experimental LOLs and simulated LOLs decrease as the temperature increases, the model overpredicts the decreasing trend. The model is more sensitive to temperature, and it is accurate with the temperature from 900 to 1100 K. For IDTs, the calculated IDTs have a good agreement with experimental data in the whole temperature range; except at 1200 K, the simulated IDT is slightly shorter than the experimental result. The maximum error of LOLs is 7.82 mm and that of IDTs is 0.16 ms, and the calculated results are basically within the experimental error band. It indicates that the present mechanism is suitable to predict the spray and ignition performance of diesel. It is worth noting that the model can mimic the diesel features well under low temperature. Under engine cold-start conditions, the diesel ignition failure and unstable flame development lead to the difficulty in engine cold starting, and also the starting process is also accompanied by a large amount of emissions. The present mechanism is proved to be further used in the development of diesel engine cold-start model and the prediction of diesel ignition performance under low temperature.

5. CONCLUSIONS

In this study, a four-component diesel surrogate fuel was developed, with the composition of *n*-hexadecane (HXN), isocetane (HMN), 1-methylnaphthalene (AMN), and *n*-butylcyclohexane (NBCH). The mechanism of surrogate fuel was validated under various conditions. Generally, the mechanism shows a satisfactory reproduction of the experimental data. Findings can be drawn as follows:

- 1) The surrogate fuel can reproduce the physicochemical characteristics of real diesel. Compared with other

surrogate fuels, the present fuel can reproduce the distillation performance of real diesel much better.

- 2) NBCH is selected as a component. The submechanism of NBCH was developed including 12 species. At high-temperature conditions, NBCH is mainly consumed through the high-temperature reaction pathway on the ring site. At low temperature, the reaction channels in the ring site and alkyl chain site are both important.
- 3) The mechanism of diesel surrogate fuel was formulated including 80 species and 251 reactions based on decoupling method and validated under a wide range of conditions with the experimental results of IDT, laminar flame speed, and species concentration of both pure components and diesel. The calculated results of IDT showed a good agreement with experimental data. The accuracy of C0–C1 submechanism needs to be improved to predict the speciation and laminar flame speed.
- 4) A diesel spray ignition test was conducted in a CVCC system under different temperatures, and the mechanism was validated with the experimental results. The calculated results showed a satisfactory agreement with the experimental data. It was proved that the mechanism is suitable to reproduce the physicochemical properties of diesel and further predict the diesel spray and ignition performance.

■ ASSOCIATED CONTENT

Supporting Information

The Supporting Information is available free of charge at <https://pubs.acs.org/doi/10.1021/acsomega.3c01540>.

Skeletal mechanism of diesel surrogate (80 species and 251 reactions) (PDF)

■ AUTHOR INFORMATION

Corresponding Authors

Zhongjie Shi – School of Mechanical Engineering, Beijing Institute of Technology, Beijing 100081, China; orcid.org/0000-0002-3822-8751; Email: shizhongjie@bit.edu.cn

Yikai Li – School of Mechanical Engineering, Beijing Institute of Technology, Beijing 100081, China; Chongqing Innovation Center, Beijing Institute of Technology, Chongqing 401120, China; Email: liyikai@bit.edu.cn

Authors

Chenghan Sun – School of Mechanical Engineering, Beijing Institute of Technology, Beijing 100081, China

Yue Lou – School of Mechanical Engineering, Beijing Institute of Technology, Beijing 100081, China

Gaoran Wei – School of Mechanical Engineering, Beijing Institute of Technology, Beijing 100081, China

Ziming Yang – School of Mechanical Engineering, Beijing Institute of Technology, Beijing 100081, China

Complete contact information is available at:

<https://pubs.acs.org/10.1021/acsomega.3c01540>

Notes

The authors declare no competing financial interest.

■ ACKNOWLEDGMENTS

This study is based on the work supported by the China Postdoctoral Science Foundation [2020M680378] and the National Natural Science Foundation of China [grant no.

51976011]. Any findings, opinions, and conclusions presented in this paper are the point of the author(s) and do not necessarily reflect the views of the funded organization.

REFERENCES

- (1) Liu, F.; Zhang, Z.; Wu, H.; Li, Y.; Ma, Y.; Li, X.; Du, W. An investigation on a diesel jet's ignition characteristics under cold-start conditions. *Appl. Therm. Eng.* **2017**, *121*, 511–519.
- (2) Liu, J.; Yao, A.; Yao, C. Effects of injection timing on performance and emissions of a HD diesel engine with DMCC. *Fuel* **2014**, *134*, 107–113.
- (3) Zhou, H.; Li, X.; Liu, F. Soot formation and oxidation mechanisms in a diesel engine separated swirl combustion system. *Fuel* **2019**, *257*, 115955.
- (4) E, J.; Xu, W.; Ma, Y.; Tan, D.; Peng, Q.; Tan, Y.; Chen, L. Soot formation mechanism of modern automobile engines and methods of reducing soot emissions: A review. *Fuel Process. Technol.* **2022**, *235*, 107373.
- (5) Wang, Q.; Sun, W.; Guo, L.; Fan, L.; Cheng, P.; Zhang, H.; Sun, Y. Effects of EGR and combustion phasing on the combustion and emission characteristic of direct-injection CI engine fueled with n-butanol/diesel blends. *Energy Procedia* **2019**, *160*, 364–371.
- (6) Fayad, M. A.; Tsolakis, A.; Martos, F. J. Influence of alternative fuels on combustion and characteristics of particulate matter morphology in a compression ignition diesel engine. *Renewable Energy* **2020**, *149*, 962–969.
- (7) Cui, Y.; Liu, H.; Wen, M.; Feng, L.; Ming, Z.; Zheng, Z.; Fang, T.; Xu, L.; Bai, X.-S.; Yao, M. Optical diagnostics of misfire in partially premixed combustion under low load conditions. *Fuel* **2022**, *329*, 125432.
- (8) Liu, H.; Cui, Y.; Chen, B.; Kyritsis, D. C.; Tang, Q.; Feng, L.; Wang, Y.; Li, Z.; Geng, C.; Yao, M. Effects of Flame Temperature on PAHs and Soot Evolution in Partially Premixed and Diffusion Flames of a Diesel Surrogate. *Energy Fuels* **2019**, *33* (11), 11821–11829.
- (9) Yu, L.; Wang, S.; Wang, W.; Qiu, Y.; Qian, Y.; Mao, Y.; Lu, X. Exploration of chemical composition effects on the autoignition of two commercial diesels: Rapid compression machine experiments and model simulation. *Combust. Flame* **2019**, *204*, 204–219.
- (10) Cui, Y.; Liu, H.; Wang, Q.; Zheng, Z.; Wang, H.; Yue, Z.; Ming, Z.; Wen, M.; Feng, L.; Yao, M. Investigation on the ignition delay prediction model of multi-component surrogates based on back propagation (BP) neural network. *Combust. Flame* **2022**, *237*, 111852.
- (11) Nageswara Rao, D.; Sreenivasulu Reddy, A. Effects on the performance and emission characteristics of CRDI diesel engine fueled with ethanol, acid oil methyl ester biodiesel and diesel blends. *Mater. Today: Proc.* **2023**, DOI: 10.1016/j.matpr.2023.06.065. In Press, Corrected Proof.
- (12) Gültekin, N.; Ciniviz, M. Experimental investigation of the effect of hydrogen ratio on engine performance and emissions in a compression ignition single cylinder engine with electronically controlled hydrogen-diesel dual fuel system. *Int. J. Hydrogen Energy* **2023**, *48*, 25984–25999.
- (13) Liu, H.; Zhang, P.; Liu, X.; Chen, B.; Geng, C.; Li, B.; Wang, H.; Li, Z.; Yao, M. Laser diagnostics and chemical kinetic analysis of PAHs and soot in co-flow partially premixed flames using diesel surrogate and oxygenated additives of n-butanol and DMF. *Combust. Flame* **2018**, *188*, 129–141.
- (14) Peng, Z.; Hai-Feng, L.; Bei-Ling, C.; Qing-Long, T.; Ming-Fa, Y. Fluorescence Spectra of Polycyclic Aromatic Hydrocarbons and Soot Concentration in Partially Premixed Flames of Diesel Surrogate Containing Oxygenated Additives. *Acta Phys. Chim. Sin.* **2015**, *31*, 32–40.
- (15) Zhang, Y.; Gao, S.; Zhang, Z.; Li, W.; Yuan, T.; Tan, D.; Duan, L.; Yang, G. A comprehensive review on combustion, performance and emission aspects of higher alcohols and its additive effect on the diesel engine. *Fuel* **2023**, *335*, 127011.
- (16) Sundar, R.; Saravanan, G. Influence of hexanol-diesel blends on constant speed diesel engine. *Therm. Sci.* **2011**, *15*, 1215–1222.
- (17) Nour, M.; Sun, Z.; El-Seesy, A. I.; Li, X. Experimental evaluation of the performance and emissions of a direct-injection compression-ignition engine fueled with n-hexanol-diesel blends. *Fuel* **2021**, *302*, 121144.
- (18) Westbrook, C. K.; Mizobuchi, Y.; Poinot, T. J.; Smith, P. J.; Warnatz, J. Computational combustion. *Proc. Combust. Inst.* **2005**, *30* (1), 125–157.
- (19) Qian, Y.; Yu, L.; Li, Z.; Zhang, Y.; Xu, L.; Zhou, Q.; Han, D.; Lu, X. A new methodology for diesel surrogate fuel formulation: Bridging fuel fundamental properties and real engine combustion characteristics. *Energy* **2018**, *148*, 424–447.
- (20) Dryer, F. L. Chemical kinetic and combustion characteristics of transportation fuels. *Proc. Combust. Inst.* **2015**, *35* (1), 117–144.
- (21) Maroteaux, F.; Noel, L. Development of a reduced n-heptane oxidation mechanism for HCCI combustion modeling. *Combust. Flame* **2006**, *146* (1–2), 246–267.
- (22) Farrell, J.; Cernansky, N.; Dryer, F.; Law, C.; Friend, D.; Hergart, C.; McDavid, R.; Patel, A.; Mueller, C.; Pitsch, H. *Development of an Experimental Database and Kinetic Models for Surrogate Diesel Fuels*; SAE Technical Papers, 2007.
- (23) Shang, W.; Cao, J.; Yang, S.; He, Z. In-flame soot quantification of N-Hexadecane droplets using diffused back-illumination extinction imaging. *Case Stud. Therm. Eng.* **2022**, *30*, 101699.
- (24) Ranzi, E.; Frassoldati, A.; Granata, S.; Faravelli, T. Wide-Range Kinetic Modeling Study of the Pyrolysis, Partial Oxidation, and Combustion of Heavy n-Alkanes. *Ind. Eng. Chem. Res.* **2005**, *44* (14), 5170–5183.
- (25) Westbrook, C. K.; Pitz, W. J.; Herbinet, O.; Curran, H. J.; Silke, E. J. A comprehensive detailed chemical kinetic reaction mechanism for combustion of n-alkane hydrocarbons from n-octane to n-hexadecane. *Combust. Flame* **2009**, *156* (1), 181–199.
- (26) Raza, M.; Mao, Y.; Yu, L.; Lu, X. Insights into the Effects of Mechanism Reduction on the Performance of n-Decane and Its Ability to Act as a Single-Component Surrogate for Jet Fuels. *Energy Fuels* **2019**, *33* (8), 7778–7790.
- (27) Ji, C.; Sarathy, S. M.; Veloo, P. S.; Westbrook, C. K.; Egolfopoulos, F. N. Effects of fuel branching on the propagation of octane isomers flames. *Combust. Flame* **2012**, *159* (4), 1426–1436.
- (28) Darcy, D.; Mehl, M.; Simmie, J. M.; Würmel, J.; Metcalfe, W. K.; Westbrook, C. K.; Pitz, W. J.; Curran, H. J. An experimental and modeling study of the shock tube ignition of a mixture of n-heptane and n-propylbenzene as a surrogate for a large alkyl benzene. *Proc. Combust. Inst.* **2013**, *34* (1), 411–418.
- (29) Mueller, C.; Cannella, W.; Bruno, T.; Bunting, B.; Dettman, H.; Franz, J.; Huber, M.; Natarajan, M.; Pitz, W.; Ratcliff, M.; et al. Methodology for Formulating Diesel Surrogate Fuels with Accurate Compositional, Ignition-Quality, and Volatility Characteristics. *Energy Fuels* **2012**, *26*, 3284–3303.
- (30) Wang, Z.; Zhao, L.; Wang, Y.; Bian, H.; Zhang, L.; Zhang, F.; Li, Y.; Sarathy, S. M.; Qi, F. Kinetics of ethylcyclohexane pyrolysis and oxidation: An experimental and detailed kinetic modeling study. *Combust. Flame* **2015**, *162* (7), 2873–2892.
- (31) Duong, L. H.; Fujita, O.; Reksowardojo, I. K.; Soerawidjaja, T. H.; Neonufa, G. F. Experimental investigation of the effects of cycloparaffins and aromatics on the sooting tendency and the freezing point of soap-derived biokerosene and normal paraffins. *Fuel* **2016**, *185*, 855–862.
- (32) Pitz, W. J.; Mueller, C. J. Recent progress in the development of diesel surrogate fuels. *Prog. Energy Combust. Sci.* **2011**, *37* (3), 330–350.
- (33) Chen, C.; Jia, P.; Chen, Y.; Tu, Z.; Deng, B.; Liu, H.; Huang, H. A multi-component surrogate mechanism of diesel from indirect coal liquefaction for diesel engine combustion and emission simulations. *Fuel* **2022**, *320*, 123928.
- (34) Wu, G.; Wang, X.; Abubakar, S.; Li, Y. A skeletal mechanism for biodiesel-dimethyl ether combustion in engines. *Fuel* **2022**, *325*, 124834.
- (35) Szymkowitz, P. G.; Benajes, J. Development of a Diesel Surrogate Fuel Library. *Fuel* **2018**, *222*, 21–34.

- (36) Szymkowitz, P. G.; Benajes, J. Single-cylinder engine evaluation of a multi-component diesel surrogate fuel at a part-load operating condition with conventional combustion. *Fuel* **2018**, *226*, 286–297.
- (37) Ranzi, E.; Frassoldati, A.; Stagni, A.; Pelucchi, M.; Cuoci, A.; Faravelli, T. Reduced Kinetic Schemes of Complex Reaction Systems: Fossil and Biomass-Derived Transportation Fuels. *Int. J. Chem. Kinet.* **2014**, *46* (9), 512–542.
- (38) Zhu, J.; Zhou, D.; Yu, L.; Qian, Y.; Lu, X. Construction of a skeletal multi-component diesel surrogate model by integrating chemical lumping and genetic algorithm. *Fuel* **2022**, *313*, 122711.
- (39) Bai, Y.; Wang, Y.; Wang, X.; Wang, P. Development of a skeletal mechanism for tri-component diesel surrogate fuel: N-hexadecane/iso-cetane/1-methylnaphthalene. *Fuel* **2020**, *259*, 116217.
- (40) Chang, Y.; Jia, M.; Li, Y.; Liu, Y.; Xie, M.; Wang, H.; Reitz, R. D. Development of a skeletal mechanism for diesel surrogate fuel by using a decoupling methodology. *Combust. Flame* **2015**, *162* (10), 3785–3802.
- (41) Kim, D.; Martz, J.; Violi, A. A surrogate for emulating the physical and chemical properties of conventional jet fuel. *Combust. Flame* **2014**, *161* (6), 1489–1498.
- (42) Mueller, C. J.; Cannella, W. J.; Bays, J. T.; Bruno, T. J.; DeFabio, K.; Dettman, H. D.; Gieleciak, R. M.; Huber, M. L.; Kweon, C.-B.; McConnell, S. S.; et al. Diesel Surrogate Fuels for Engine Testing and Chemical-Kinetic Modeling: Compositions and Properties. *Energy Fuels* **2016**, *30* (2), 1445–1461.
- (43) Pitz, W.; Liang, J.; Kukkadapu, G.; Zhang, K.; Conroy, C.; Bugler, J.; Curran, H. J. A detailed chemical kinetic modeling and experimental investigation of the low- and high-temperature chemistry of n-butylcyclohexane. *Int. J. Chem. Kinet.* **2021**, *53*, 465–475.
- (44) Mao, Y.; Li, A.; Zhu, L.; Wu, Z.; Yu, L.; Wang, S.; Raza, M.; Lu, X. A detailed chemical mechanism for low to high temperature oxidation of n-butylcyclohexane and its validation. *Combust. Flame* **2019**, *210*, 360–373.
- (45) Edwards, T.; Colket, M.; Cernansky, N.; Dryer, F.; Egolfopoulos, F.; Friend, D.; Law, E.; Lenhart, D.; Lindstedt, P.; Pitsch, H.; et al. Development of an Experimental Database and Kinetic Models for Surrogate Jet Fuels. *AIAA* **2007**, *14*, DOI: 10.2514/6.2007-770.
- (46) Chang, Y.; Jia, M.; Liu, Y.; Li, Y.; Xie, M. Development of a new skeletal mechanism for n-decane oxidation under engine-relevant conditions based on a decoupling methodology. *Combust. Flame* **2013**, *160* (8), 1315–1332.
- (47) Ranzi, E.; Frassoldati, A.; Grana, R.; Cuoci, A.; Faravelli, T.; Kelley, A. P.; Law, C. K. Hierarchical and comparative kinetic modeling of laminar flame speeds of hydrocarbon and oxygenated fuels. *Prog. Energy Combust. Sci.* **2012**, *38* (4), 468–501.
- (48) Wang, H.; Warner, S. J.; Oehlschlaeger, M. A.; Bounaceur, R.; Biet, J.; Glaude, P.-A.; Battin-Leclerc, F. An experimental and kinetic modeling study of the autoignition of α -methylnaphthalene/air and α -methylnaphthalene/n-decane/air mixtures at elevated pressures. *Combust. Flame* **2010**, *157* (10), 1976–1988.
- (49) Oehlschlaeger, M. A.; Steinberg, J.; Westbrook, C. K.; Pitz, W. J. The autoignition of iso-cetane at high to moderate temperatures and elevated pressures: Shock tube experiments and kinetic modeling. *Combust. Flame* **2009**, *156* (11), 2165–2172.
- (50) Sarathy, S. M.; Westbrook, C. K.; Mehl, M.; Pitz, W. J.; Togbe, C.; Dagaut, P.; Wang, H.; Oehlschlaeger, M. A.; Niemann, U.; Seshadri, K.; et al. Comprehensive chemical kinetic modeling of the oxidation of 2-methylalkanes from C7 to C20. *Combust. Flame* **2011**, *158* (12), 2338–2357.
- (51) Klippenstein, S. J.; Harding, L. B.; Davis, M. J.; Tomlin, A. S.; Skodje, R. T. Uncertainty driven theoretical kinetics studies for CH₃OH ignition: HO₂+CH₃OH and O₂+CH₃OH. *Proc. Combust. Inst.* **2011**, *33* (1), 351–357.
- (52) Patel, A.; Kong, S.-C.; Reitz, R. *Development and Validation of a Reduced Reaction Mechanism for HCCI Engine Simulations*. SAE Paper 2004-01-0558; SAE Technical Papers, 2004.
- (53) Mao, Y.; Yu, L.; Qian, Y.; Wang, S.; Wu, Z.; Raza, M.; Zhu, L.; Hu, X.; Lu, X. Development and validation of a detailed kinetic model for RP-3 aviation fuel based on a surrogate formulated by emulating macroscopic properties and microscopic structure. *Combust. Flame* **2021**, *229*, 111401.
- (54) Naik, C. V.; Puduppakkam, K. V.; Modak, A.; Meeks, E.; Wang, Y. L.; Feng, Q.; Tsotsis, T. T. Detailed chemical kinetic mechanism for surrogates of alternative jet fuels. *Combust. Flame* **2011**, *158* (3), 434–445.
- (55) Wang, Q.; Chen, C. P. Simulated Kinetics and Chemical and Physical Properties of a Four-Component Diesel Surrogate Fuel. *Energy Fuels* **2017**, *31* (12), 13190–13197.
- (56) Pitz, W. J.; Liang, J.; Kukkadapu, G.; Zhang, K.; Conroy, C.; Bugler, J.; Curran, H. J. A detailed chemical kinetic modeling and experimental investigation of the low- and high-temperature chemistry of n-butylcyclohexane. *Int. J. Chem. Kinet.* **2021**, *53* (3), 465–475.
- (57) Pitz, W. J.; Conroy, C.; Bugler, J.; Curran, H. J. An Experimental and Modeling Study of the Autoignition of n-Butylcyclohexane over a Wide Pressure, Temperature and Equivalence-Ratio Range. United States, 2015-03-10, 2015; Research Org.: Lawrence Livermore National Lab. (LLNL), Livermore, CA (United States), Sponsor Org.: USDOE. DOI: Conference: Presented at. 9th U. S. National Combustion Meeting: Cincinnati, OH, United States, June 17–June 20, 2015.
- (58) Natelson, R. H.; Kurman, M. S.; Cernansky, N. P.; Miller, D. L. Low temperature oxidation of n-butylcyclohexane. *Combust. Flame* **2011**, *158* (12), 2325–2337.
- (59) Mao, Y.; Wang, S.; Wu, Z.; Qiu, Y.; Yu, L.; Ruan, C.; Chen, F.; Zhu, L.; Lu, X. An experimental and kinetic modeling study of n-butylcyclohexane over low-to-high temperature ranges. *Combust. Flame* **2019**, *206*, 83–97.
- (60) Chang, Y.; Jia, M.; Liu, Y.; Li, Y.; Xie, M.; Yin, H. Application of a Decoupling Methodology for Development of Skeletal Oxidation Mechanisms for Heavy n-Alkanes from n-Octane to n-Hexadecane. *Energy Fuels* **2013**, *27* (6), 3467–3479.
- (61) Sun, X.; Liang, X.; Yu, H.; Wang, Y.; Zhu, Z. Comparison the Performance of N-heptane, N-dodecane, N-tetradecane and N-hexadecane. *Energy Procedia* **2017**, *105*, 1426–1433.
- (62) Kukkadapu, G.; Sung, C.-J. Autoignition Study of 1-Methylnaphthalene in a Rapid Compression Machine. *Energy Fuels* **2017**, *31* (1), 854–866.
- (63) Gowdagiri, S.; Wang, W.; Oehlschlaeger, M. A. A shock tube ignition delay study of conventional diesel fuel and hydroprocessed renewable diesel fuel from algal oil. *Fuel* **2014**, *128*, 21–29.
- (64) Yu, L.; Mao, Y.; Li, A.; Wang, S.; Qiu, Y.; Qian, Y.; Han, D.; Zhu, L.; Lu, X. Experimental and modeling validation of a large diesel surrogate: Autoignition in heated rapid compression machine and oxidation in flow reactor. *Combust. Flame* **2019**, *202*, 195–207.
- (65) Mati, K.; Ristori, A.; Gail, S.; Pengloan, G.; Dagaut, P. The oxidation of a diesel fuel at 1–10 atm: Experimental study in a JSR and detailed chemical kinetic modeling. *Proc. Combust. Inst.* **2007**, *31* (2), 2939–2946.
- (66) Li, B.; Liu, N.; Zhao, R.; Zhang, H.; Egolfopoulos, F. N. Flame propagation of mixtures of air with high molecular weight neat hydrocarbons and practical jet and diesel fuels. *Proc. Combust. Inst.* **2013**, *34* (1), 727–733.
- (67) Pickett, L.; Kook, S.; Williams, T. Visualization of Diesel Spray Penetration, Cool-Flame, Ignition, High-Temperature Combustion, and Soot Formation Using High-Speed Imaging. *SAE International Journal of Engines* **2009**, *2*, 439–459.
- (68) Lillo, P.; Pickett, L.; Persson, H.; Andersson, O.; Kook, S. Diesel Spray Ignition Detection and Spatial/Temporal Correction. *SAE International Journal of Engines* **2012**, *5*, 1330–1346.
- (69) Pickett, L.; Siebers, D.; Idicheria, C. *Relationship Between Ignition Processes and the Lift-Off Length of Diesel Fuel Jets*; SAE Technical Papers, 2005.
- (70) Yang, Z.; Lee, T. H.; Li, Y.; Chen, W.-T.; Zhang, Y. Spray and combustion characteristics of pure hydrothermal liquefaction biofuel and mixture blends with diesel. *Fuel* **2021**, *294*, 120498.
- (71) Pei, Y.; Som, S.; Pomraning, E.; Senecal, P. K.; Skeen, S. A.; Manin, J.; Pickett, L. M. Large eddy simulation of a reacting spray flame

with multiple realizations under compression ignition engine conditions. *Combust. Flame* **2015**, *162* (12), 4442–4455.

(72) Pomraning, E. Development of Large Eddy Simulation Turbulence Models. Ph.D. Dissertation, Madison ProQuest Dissertations Publishing, 2000.

(73) Reitz, R. D.; Bracco, F. V. Mechanisms of breakup of round liquid jets. *Encyclopedia of Fluid Mechanics* **1986**, *3*, 223.

(74) Ricart, L. M.; Xin, J.; Bower, G. R.; Reitz, R. *In-Cylinder Measurement and Modeling of Liquid Fuel Spray Penetration in a Heavy-Duty Diesel Engine*; SAE Technical Papers, 1997.

(75) Senecal, P.; Pomraning, E.; Richards, K.; Briggs, T.; Choi, C.; McDavid, R.; Patterson, M. *Multi-Dimensional Modeling of Direct-Injection Diesel Spray Liquid Length and Flame Lift-off Length using CFD and Parallel Detailed Chemistry*; SAE Technical Papers, 2003.

(76) Skeen, S. A.; Manin, J.; Pickett, L. M. Simultaneous formaldehyde PLIF and high-speed schlieren imaging for ignition visualization in high-pressure spray flames. *Proc. Combust. Inst.* **2015**, *35*, 3167–3174.

(77) Wang, Z. K.; Stamatoglou, P.; Lundgren, M.; Luise, L.; Vaglieco, B. M.; Andersson, A.; Alden, M.; Andersson, O.; Richter, M. Simultaneous 36 kHz PLIF/chemiluminescence imaging of fuel, CH₂O and combustion in a PPC engine. *Proc. Combust. Inst.* **2019**, *37* (4), 4751–4758.

(78) Sim, H. S.; Maes, N.; Weiss, L.; Pickett, L. M.; Skeen, S. A. Detailed measurements of transient two-stage ignition and combustion processes in high-pressure spray flames using simultaneous high-speed formaldehyde PLIF and schlieren imaging. *Proc. Combust. Inst.* **2021**, *38* (4), 5713–5721.

(79) Krisman, A.; Hawkes, E. R.; Talei, M.; Bhagatwala, A.; Chen, J. H. Characterisation of two-stage ignition in diesel engine-relevant thermochemical conditions using direct numerical simulation. *Combust. Flame* **2016**, *172*, 326–341.

(80) Dalakoti, D. K.; Savard, B.; Hawkes, E. R.; Wehrfritz, A.; Wang, H.; Day, M. S.; Bell, J. B. Direct numerical simulation of a spatially developing n-dodecane jet flame under Spray A thermochemical conditions: Flame structure and stabilisation mechanism. *Combust. Flame* **2020**, *217*, 57–76.